$NaPN_2$: Deep-ultraviolet nonlinear optical material with unprecedented strong second-harmonic generation coefficient

Zhi Li,[1] Abudukadi Tudi,[1,2] Peng Ren,[1,2] Yun Yang,[1] Toshiaki Iitaka,[3] Takami Tohyama,[4] Zhihua Yang,[1,*] Shilie Pan,[1,†] and Haibin Su[5,‡]

[1]*Key Laboratory of Functional Materials and Devices for Special Environments of CAS, Xinjiang Technical Institute of Physics and Chemistry of CAS, Xinjiang Key Laboratory of Electronic Information Materials and Devices, 40-1 South Beijing Road, Urumqi 830011, China*

[2]*University of Chinese Academy of Sciences, Beijing 100049, China*

[3]*Computational Astrophysics Laboratory, RIKEN, 2-1 Hirosawa, Wako, Saitama 351-0198, Japan*

[4]*Department of Applied Physics, Tokyo University of Science, Katsushika, Tokyo 125-8585, Japan*

[5]*Department of Chemistry, The Hong Kong University of Science and Technology, Hong Kong, China*

(Received 6 April 2018; published 19 February 2019)

The electronic band structures and second harmonic generations (SHGs) of phosphorus nitrides $LiPN_2$, $NaPN_2$, and $CuPN_2$ are studied by first-principles calculations. $NaPN_2$ has a band gap of ~6.2 eV (200 nm) and the strongest SHG coefficient among phosphorus-based deep-ultraviolet nonlinear optical (NLO) materials, i.e., $d_{36} = 2.35$ pm/V at static limit and $d_{36} = 3.77$ pm/V under external optic field with wavelength 1064 nm. Compared with the SHG coefficients of borate NLO materials working in the region of deep ultraviolet, $NaPN_2$ presents an unprecedented high SHG coefficient, which is the manifestation of its enhanced orbital hybridization owing to the shorter bond lengths from high pressure facilitated synthesis.

DOI: 10.1103/PhysRevMaterials.3.025201

I. INTRODUCTION

Coherent deep-ultraviolet (DUV, wavelength $\lambda < 200$ nm) light sources play a pivotal role in enabling a wide range of important technologies, including imaging, spectroscopy, optical communications, etc. [1–5]. The core part of a coherent DUV light source is built on frequency conversion by nonlinear optical (NLO) materials [6], which should satisfy the following requirements: broken spatial inversion symmetry, a band gap larger than 6.2 eV for a wide transparency window in the DUV region, relatively large second harmonic generation (SHG) coefficient (larger than the SHG coefficient of KH_2PO_4, i.e., 0.39 pm/V under optic field with wavelength 1064 nm), and sufficient birefringence to ensure phase matching in the DUV wavelength range [7]. The widely used NLO borate crystals LiB_3O_5 [8], β-BaB_2O_4 [9], and $KBe_2BO_3F_2$ (KBBF) are featured by relatively strong SHG coefficient with moderate birefringence. For instance, KBBF has a DUV cutoff wavelength 150 nm, exhibiting appreciable SHG of $d_{11} = 0.47$ pm/V under optic field with wavelength 1064 nm with a rather moderate birefringence value of 0.077; it is a popular NLO material to generate laser light with wavelengths in the DUV region [10]. However, considering all NLO borates with band gap larger than 6.2 eV, none of them has a SHG coefficient larger than 2.5 pm/V under optic field with wavelength 1064 nm [7]; the notable $Sr_2Be_2B_2O_7$ has the highest SHG coefficient of 2.48 pm/V under optic field with wavelength 1064 nm with a band gap of ~8.0 eV [11]. The SHG coefficients of recently synthesized borate fluorides, such as $NH_4B_4O_6F$ [12], RbB_4O_6F [13], and CsB_4O_6F [14], are all even below 1.2 pm/V under optic field with wavelength 1064 nm.

The SHG coefficient at static limit is considered to be proportional to the inverse of band gap [15]. NLO materials with relatively small band usually present high SHG coefficient. For example, Weyl semimetal TaAs with zero band gap presents a very large SHG coefficient of $d_{33} = 3600$ pm/V under optic field with wavelength 800 nm [16]. In contrast to this widely accepted scenario, BPO_4 exhibits a larger SHG coefficient, $d_{36} = 0.76$ pm/V, than that of KBBF, i.e., $d_{11} = 0.47$ pm/V, even though the band gap of BPO_4 (~9.25 eV) is wider than that of KBBF (~8.43 eV) [17]. This intriguing observation indicates that it is insufficient to understand the SHG from band gap value exclusively. Therefore, the contributions from both charge transfer and orbital hybridization to the band gap should be considered explicitly when we analyze the microscopic origin of the SHG's variance. For instance, the enhanced orbital hybridization by external pressure can enhance the SHG coefficient in insulators with large charge transfer energy [15]. Considering that materials synthesized under high pressure conditions usually present much stronger orbital hybridization, we propose to investigate SHG coefficients of phosphorus nitrides $NaPN_2$ and $CuPN_2$, which can be synthesized under high pressure and high temperature [18–20]. From first-principles calculations, we report an unprecedented high SHG coefficient among phosphorus based DUV NLO materials, $d_{36} = 3.77$ pm/V under optic field with wavelength 1064 nm in phosphorus nitride $NaPN_2$ with a band gap of ~6.2 eV.

*zhyang@ms.xjb.ac.cn
†slpan@ms.xjb.ac.cn
‡haibinsu@ust.hk

II. COMPUTATIONAL METHOD

For the electronic structure, first-principles calculations based on density functional theory were carried out within a primitive cell with a $28 \times 28 \times 28$ k-point grid and 500 eV energy cutoff. Projector augmented wave pseudopotentials with Perdew, Burke, and Ernzerhof (PBE) exchange correlation are adopted in our calculation [21–23]. Since PBE exchange correlation may underestimate the band gap, we also performed calculations employing the all-electron, full-potential linearized augment plane wave (FPLAPW) method with the modified Becke and Johnson local density approximation (MBJLDA) implemented in WIEN2K code [24,25]. For the frequency dependent SHG coefficient, a first-principles calculation with sum-over-state (SOS) approximation is performed with a scissor determined by the band gap difference from PBE calculation and MBJLDA calculation [26–30], respectively. All studied phosphorus nitrides here crystalize into tetragonal crystal structure with I-42d space group. Experimental structural parameters are adopted [18–20], and geometry optimization is not performed [31]. In the self-consistent calculation, the tolerances for wave function squared residual and energy difference are less than 1.0×10^{-20} and 1.0×10^{-12} hartree/cell, respectively. The energy cut for plane wave is 20 hartree.

III. ELECTRONIC STRUCTURES

In the borate NLO crystals, BPO_4 has both larger band gap and SHG coefficient than those of KBBF. It indicates that SHG coefficient is not determined by the band gap of noncentrosymmetric material exclusively. In our previous work [15], we concluded that strong SHG in an insulator with almost flat band structure is dominated by the appreciable orbital hybridization, which is tunable under external pressure. As materials synthesized under high pressure present shorter bond length and stronger orbital hybridization, here we choose two materials from high pressure facilitated synthesis, $NaPN_2$ and $CuPN_2$, to study their electronic structures and SHGs by first-principles calculations. Although high pressure is not needed to make $LiPN_2$, which can be synthesized at high temperature [18], considering the close relation in terms of structural aspect, we also include $LiPN_2$ in this work.

The calculated band structures of $LiPN_2$, $NaPN_2$ and $CuPN_2$ are shown in Fig. 1. The band gap of $NaPN_2$ is about 6.2(4.7) eV from MBJLDA (PBE) calculation. The

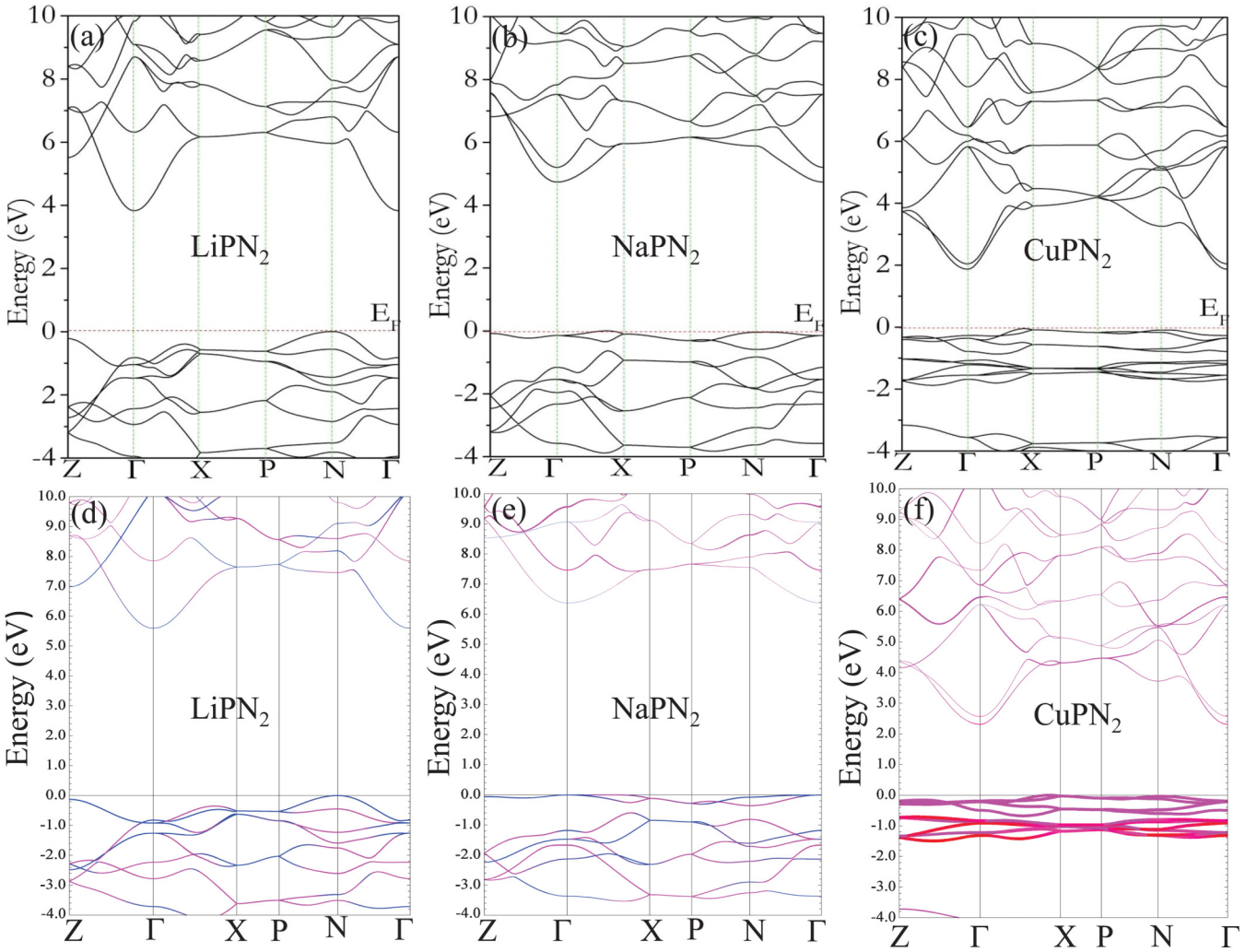

FIG. 1. The calculated band structures of $LiPN_2$, $NaPN_2$, and $CuPN_2$ by first-principles calculation with PBE (a)–(c) and MBJLDA (d)–(f). The weights of p orbitals of N and s (d) orbitals of Li/Na (Cu) are in blue and red, respectively.

band gap of $LiPN_2$ is about 5.5(3.8) eV from MBJLDA (PBE) calculation, while the band gap of $CuPN_2$ is only 2.3(1.5) eV from MBJLDA (PBE) calculation. In the calculated band structures from MBJLDA calculation, as shown in Figs. 1(d) and 1(f), we also mark the weight of $2p$ orbitals of N in blue, and s (d) orbitals from both Li/Na (Cu) in red, respectively. The calculated band structures reveal that the valence bands just below the Fermi level are dominated by the $2p$ orbitals of N, which are strongly hybridized with the s (d) orbitals from P and Li/Na (Cu). In all calculated band structures, the valence band below the Fermi level is minutely dispersive. Especially, the conducting band of $NaPN_2$ is less dispersive because of long Na-Na distance. The small band gap of $CuPN_2$ can be interpreted by the small charge transfer energy between $3d$ orbitals of Cu and $2p$ orbitals of N.

The light-matter coupling can be described by the following model Hamiltonian in length gauge [32,33]:

$$H(\mathbf{k},t) = h_0(\mathbf{k}) + H_1 = h_0(\mathbf{k}) - e\mathbf{r}\cdot E(t), \tag{1}$$

where $h_0(\mathbf{k})$ is the momentum-dependent unperturbed Hamiltonian, and $E(t) = E(\omega)e^{-i\omega t}$ is a time-dependent external electric field. For the intrinsic NLO effect from band structure, we ignore all the scattering terms here. With orthogonal Bloch wave functions $|n\rangle = e_n(\mathbf{k},\mathbf{r})$ satisfying $h_0(\mathbf{k})e_n(\mathbf{k}) = \epsilon_n e_n(\mathbf{k})$, the solution for Hamiltonian (1) can be expressed as

$$|\psi(\mathbf{r})\rangle = \int_{\mathrm{BZ}} \frac{d^3\mathbf{k}}{(2\pi)^3} a_n(\mathbf{k}) e_n(\mathbf{k},\mathbf{r}), \tag{2}$$

where n is band index, and momentum takes values in whole Brillouin zone (BZ). The density matrix ρ is defined as

$$\rho(\mathbf{k},t) = C_n^*(\mathbf{k},t)C_m(\mathbf{k},t)|e_n\rangle\langle e_m|. \tag{3}$$

The dynamics of $\rho(\mathbf{k},t)$ can be described by the collisionless quantum kinetic equation [34,35]

$$-\hbar\frac{\partial\rho(\mathbf{k},t)}{\partial t} = e\mathbf{E}\cdot\frac{\partial\rho(\mathbf{k},t)}{\partial\mathbf{k}} + i[H,\rho(\mathbf{k},t)]. \tag{4}$$

The first-order interband ($n \neq m$) density matrix reads

$$\rho^{(1)}_{nm}(\mathbf{k},\omega) = \frac{\langle n|H_1|m\rangle\left(\rho^{(0)}_{mm} - \rho^{(0)}_{nn}\right)}{\hbar\omega - \epsilon_{nm}(\mathbf{k})}. \tag{5}$$

For a large band gap insulator, $\rho^{(0)}_{nn}$ is 1.0 (0.0) for the valence (conduction) band. Since k_BT (k_B denotes Boltzmann constant, T temperature) is much smaller than the large band gap of insulators, we ignore the temperature effect from the Fermi-Dirac distribution for simplicity. The first-order intraband density matrix is always vanishing. The second-order density matrix $\rho^{(2)} \propto E^2$. Making use of the definition of the position operator in the Bloch state $\langle n|\mathbf{r}|m\rangle = \mathbf{a}_{nm}(\mathbf{k}) - i\delta_{nm}\partial_{\mathbf{k}}$ and $\mathbf{a}_{nm}(\mathbf{k}) = i\langle n|\partial_{\mathbf{k}}|m\rangle$ [36–39], the second-order intraband and interband density matrices read

$$\rho^{(2)}_{nn}(2\omega) = \sum_m \frac{\langle n|H_1|m\rangle\rho^{(1)}_{mn} - \rho^{(1)}_{nm}\langle m|H_1|n\rangle}{2\hbar\omega}, \tag{6}$$

$$\rho^{(2)}_{nm}(2\omega) = \frac{eE(\omega)}{2\hbar\omega - \epsilon_{nm}}\left(-i\frac{\partial}{\partial k} + \mathbf{a}_{mm} - \mathbf{a}_{nn}\right)\rho^{(1)}_{nm} + \sum_{l\neq n, l\neq m}\frac{\langle n|H_1|l\rangle\rho^{(1)}_{lm} - \rho^{(1)}_{nl}\langle l|H_1|m\rangle}{2\hbar\omega - \epsilon_{nm}}, \tag{7}$$

respectively. The secondorder electronic polarization along the y direction is determined by

$$P^{(2)}_y = e\sum_n \langle n|y\rho^{(2)}|n\rangle = \sum_{nl}\langle n|y|l\rangle\langle l|\rho^{(2)}|n\rangle. \tag{8}$$

For $n = l$, the intraband current $P^{(2)}_{inj}(2\omega)$ along the y direction reads

$$P^{(2)}_{y,I}(2\omega) = e\sum_n\int_{\mathrm{BZ}}\frac{d\mathbf{k}}{(2\pi)^3}\langle n|y|n\rangle\rho^{(2)}_{nn}(\mathbf{k},\omega) = \frac{-e^2E(\omega)}{2\hbar\omega}\sum_{n\neq m}\int_{\mathrm{BZ}}\frac{d\mathbf{k}}{(2\pi)^3}a_{mn}D^y_{nm}\rho^{(1)}_{nm}, \tag{9}$$

and the interband electronic polarization reads

$$P^{(2)}_{y,T}(2\omega) = \sum_{nm}\int_{\mathrm{BZ}}\frac{d\mathbf{k}}{(2\pi)^3}\frac{e^2E(\omega)\langle m|y|n\rangle}{2\hbar\omega - \epsilon_{nm}}D^x_{nm}\rho^{(1)}_{nm}. \tag{10}$$

Here, we ignored the contribution involving three bands, i.e., the second term in Eq. (7) is omitted. The justification for such treatment is that $\langle m|y|l\rangle\langle l|H_1|n\rangle\rho^{(1)}_{nm}$ does not vanish only when the three atomic orbital hybridize with each other, i.e., three-body interaction is usually weaker than two-body interaction. The vector $\mathbf{D}_{nm}(\mathbf{k}) = -i\partial_{\mathbf{k}} + \mathbf{a}_{mm}(\mathbf{k}) - \mathbf{a}_{nn}(\mathbf{k})$, which characterizes the difference between intracell position matrices within valence and conduction bands, is gauge invariant under the local phase transformation of the Bloch function. The shift vector defined in momentum space is analogous to the dipole in real space [40]. Both Eqs. (9) and (10) are locally gauge invariant if we multiply any function $\exp[i\theta(\mathbf{k})]$ by the Bloch function of the unperturbed ground state. Importantly, the shift vector $D(\mathbf{k})$ is explicitly presented in Both Eqs. (9) and (10), in which both shift vector and gauge invariance are incorporated. From Eqs. (9) and (10), we conclude that shift vector is the unique source for NLO susceptibility in a noncentrosymmetric insulator [41–48], even though there are several channels for SHG in metal [49–52]. Except for the shift vector, the SHG coefficient is also related to the interband Berry connection $a_{nm}(\mathbf{k})$, which characterizes the possibility of transition between energy bands $|n(\mathbf{k})\rangle$ and $|m(\mathbf{k})\rangle$. In the case of large charge transfer energy, the interband Berry connection $a_{nm}(\mathbf{k})$ can be enhanced by strong orbital hybridization [15], i.e., bond covalency [53]. External pressure can reduce the bond length and enhance the overlapping of atomic orbitals. Additionally, we can enhance the shift vector by large atomic displacement, which breaks spatial inversion symmetry [54].

Since all studied materials here are large band gap insulators and are topologically trivial, the NLO response here is exclusively determined by the shift vector mechanism. We calculated the SHG coefficients of $LiPN_2$, $NaPN_2$, and $CuPN_2$ contributed by the shift vector mechanism by the SOS approximation implemented in the ABINIT code [28]. Since PBE approximation always underestimates the band gap of NLO crystals [15], a scissor operator at 1.7, 1.5, and 0.8 eV is adopted for $LiPN_2$, $NaPN_2$, and $CuPN_2$, respectively, to enlarge band gap artificially in all calculations. Here, the scissor operator takes the band gap difference of each material calculated by PBE approximation and MBJLDA, respectively, and it will be added to the eigenvalues of each conducting

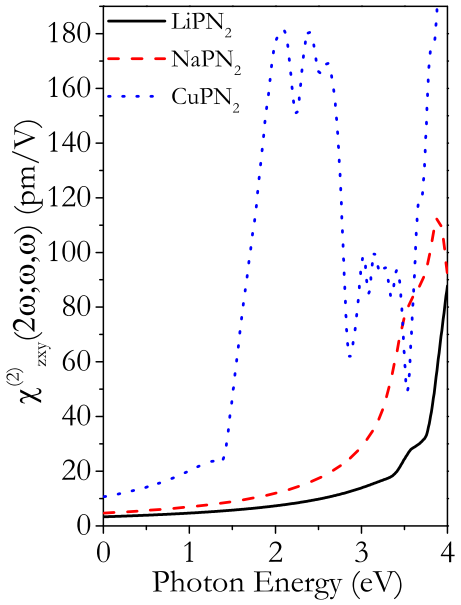

FIG. 2. The calculated photon energy dependent SHG $\chi^{(2)}_{zxy}(2\omega;\omega,\omega)$ by first-principles calculation with SOS approximation and scissor correction determined by the band gap difference between PBE and MBJLDA calculations.

band. By calculation, the $d_{36} = \frac{1}{2}\chi^{(2)}_{zxy}(2\omega;\omega,\omega)$ coefficient in each material presents the largest component value. In the region of low frequency, the calculated frequency dependent SHG coefficients are very flat, as shown in Fig. 2. Before the two-photon resonance, the SHG coefficients increase slightly with the increase of photon energy. This consistency indicates that the physics at low frequency is captured in the two-band model proposed in our previous work [15]. At static limit, d_{36} of $NaPN_2$ ($LiPN_2$) is about 2.35 (1.67) pm/V. Under optic field with wavelength 1064 nm, the d_{36} coefficient is about 3.77 pm/V, which is larger than the SHG coefficient of any discovered NLO crystal working in the DUV region, i.e., the band gap is larger than 6.2 eV. Experimentally, borate NLO material $Sr_2Be_2B_2O_7$ has a band gap of about 8.0 eV and a relatively large SHG coefficient $d_{22} = 2.48$ pm/V under optic field with wavelength 1064 nm [11]. The calculated SHG coefficient of $Sr_2Be_2B_2O_7$ is unavailable because of the structural instability of $Sr_2Be_2B_2O_7$. Commercially available β-BaB_2O_4 has a band gap of about 6.7 eV and a large SHG coefficient $d_{22} = 2.2 \pm 0.05$ pm/V by experimental measurement [55]. By first-principles calculation, the calculated SHG coefficient $d_{22} = 2.03$ pm/V by Lin *et al.* [56,57] and 2.98 pm/V by Duan *et al.* [58]. In the NLO materials working in the DUV region, β-BaB_2O_4 has the largest SHG coefficient. BPO_4 has the same space group as $NaPN_2$, but it has relatively small $d_{36} = 0.74$ pm/V because of the large band gap. From our calculation, $NaPN_2$ synthesized under high pressure presents larger SHG coefficient than that of β-BaB_2O_4, although the growth of single crystals under high pressure may be challenging. Anyway, high pressure affords a simple method to enhance SHG coefficient by enhancing bond covalency.

Even though $NaPN_2$ has a larger band gap than $LiPN_2$, the SHG coefficient d_{36} of $NaPN_2$ is also larger. $NaPN_2$ synthesized under high pressure has relatively short N-P bond length 1.639 Å, while N-P bond length in $LiPN_2$ is 1.644 Å. In contrast to the relatively long Li-N bond length 2.093 Å in $LiPN_2$, the Na-N bond length in $NaPN_2$ is slightly elongated to 2.409 Å, because 3*s* orbitals of Na are more spatially extended. Since the Li-P (Na-P) bond length in $LiPN_2$ ($NaPN_2$) is larger than 3.0 Å, the orbital hybridization between Li-P (Na-P) is ignorable. From the band structures of $LiPN_2$ and $NaPN_2$, the *sp* hybridization between Li-N and Na-N is obvious. Since the charge transfer energy between 3*s*-Na and 2*p*-N is lower than that between 2*s*-Li and 2*p*-N, the larger band gap of $NaPN_2$ can be interpreted by the relatively strong *sp* hybridization between 3*s*-Na and 2*p*-N. In contrast to $LiPN_2$, the larger SHG coefficient in $NaPN_2$ can be interpreted by the enhanced orbital hybridization between 3*s*-Na and 2*p*-N. The slightly reduced N-P bond length in $NaPN_2$ can also enhance the NLO response somewhat. The large SHG coefficient d_{36} of $CuPN_2$ can be simply interpreted as the reduced band gap. The reduced band gap mainly results from the relatively low charge transfer energy between 3*d*-Cu and 2*p*-N. Even though d_{36} of $CuPN_2$ is as large as 5.35 pm/V, it cannot work in the DUV region because of its small band gap, 2.3 eV.

Moderate birefringence Δn is another criterion for an excellent NLO crystal. For phase matching in the DUV region, Δn should be larger than 0.07 and smaller than 0.1. We also calculated the birefringence of $LiPN_2$ and $NaPN_2$ by first-principles calculation with the same computational parameters as in the SHG calculation. At static limit, both $LiPN_2$ and $NaPN_2$ present relatively small birefringence, as shown in Fig. 3. The calculated birefringence of $NaPN_2$ at input wavelength 1064 nm is slightly smaller than that of LiB_3O_5 [59–61]. The small Δn of $NaPN_2$ can be interpreted by its weak anisotropy of the crystal, while the large Δn in KBBF results from the layered structure, which also reins in the growth of single crystals with large size. The calculated frequency-dependent birefringence of $NaPN_2$ ($LiPN_2$)

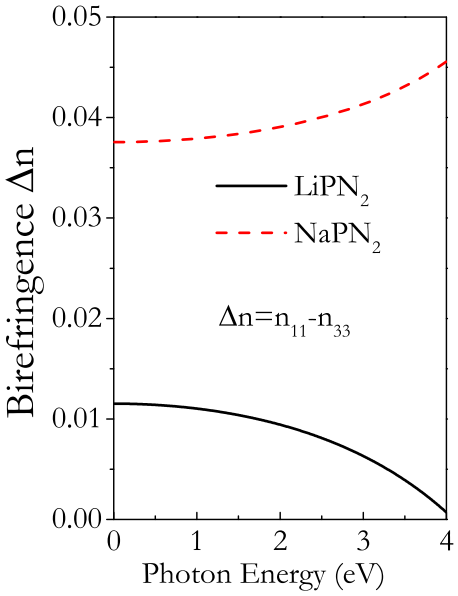

FIG. 3. Calculated photon energy-dependent birefringence by first-principles calculation.

is increasing (decreasing) slightly with the increase of frequency of incident photons. Quasi-phase-matching technology may be required to optimize the output power of laser light.

IV. SUMMARY

In summary, our computations by first principles method reveal that $NaPN_2$ has a remarkable band gap ~6.2 eV (200 nm) and the strongest SHG among phosphorus based DUV NLO materials, $d_{36} = 2.35$ pm/V at static limit and $d_{36} = 3.77$ pm/V under external optic field with wavelength 1064 nm. Compared to the SHG coefficients of borate nonlinear optical (NLO) materials working in the region of deep ultraviolet, $NaPN_2$ presents an unprecedented high SHG coefficient, which can be interpreted by its enhanced orbital hybridization due to shorter bond lengths from the high pressure facilitated synthesis.

ACKNOWLEDGMENTS

This work is supported by the National Basic Research Program of China (Grant No. 2014CB648400), the National Natural Science Foundation of China (Grant No. 51425206), the Recruitment Program of Global Experts (Thousand Talent Plan, Xinjiang Special Program), and the Director Foundation of XTIPC, CAS (Grant No. 2016RC001). T.T. and T.I. are supported by MEXT via Exploratory Challenge on Post-K Computer (Frontiers of Basic Science: Challenging the Limits). The calculations were performed on the Hokusai system (Project No. Q18231) of RIKEN. H.B.S. is grateful for support from the Society of Interdisciplinary Research (SOIREE).

[1] N. Savage, Nat. Photonics **1**, 83 (2007).
[2] J. Meng *et al.*, Nature (London) **462**, 335 (2009).
[3] T. Sekikawa, A. Kosuge, T. Kanai, and S. Watanabe, Nature (London) **432**, 605 (2004).
[4] D. F. Eaton, Science **253**, 281 (1991).
[5] Y. R. Shen, Nature (London) **337**, 519 (1989).
[6] R. W. Boyd, *Nonlinear Optics*, 3rd ed. (Elsevier, New York, 2008).
[7] T. T. Tran, H. Yu, J. M. Rondinelli, K. R. Poeppelmeier, and P. S. Halasyamani, Chem. Mater. **28**, 5238 (2016).
[8] Y. C. Wu, A. D. Jiang, S. F. Lu, C. T. Chen, and Y. S. Shen, J. Synth. Cryst. **19**, 33 (1990).
[9] C. C. Chen, T. Sasaki, R. K. Li, Y. Wu, Z. Lin, Y. Mori, Z. Hu, J. Wang, S. Uda, M. Yoshimura, and Y. Kaneda, *Nonlinear Optical Borate Crystals: Principals and Applications* (Wiley, New York, 2012).
[10] Y. N. Xia, C. T. Chen, D. Y. Tang, and B. C. Wu, Adv. Mater. **7**, 79 (1995).
[11] C. Chen, Y. Wang, B. Wu, K. Wu, W. Zeng, and L. Yu, Nature (London) **373**, 322 (1995).
[12] G. Shi, Y. Wang, F. Zhang, B. Zhang, Z. Yang, X. Hou, S. Pan, and K. R. Poeppelmeier, J. Am. Chem. Soc. **139**, 10645 (2017).
[13] X. Wang, Y. Wang, B. Zhang, F. Zhang, Z. Yang, and S. Pan, Angew. Chem. Int. Ed. **56**, 14119 (2017).
[14] Y. Wang, B. Zhang, Z. Yang, and S. Pan, Angew. Chem. Int. Ed. **57**, 2150 (2018).
[15] Z. Li, Q. Liu, Y. Wang, T. Iitaka, H. Su, T. Tohyama, Z. Yang, and S. Pan, Phys. Rev. B **96**, 035205 (2017).
[16] L. Wu, S. Patankar, T. Morimoto, N. L. Nair, E. Thewalt, A. Little, J. A. Analytis, J. E. Moore, and J. Orenstein, Nat. Phys. **13**, 350 (2017).
[17] Z. Li, Z. Lin, Y. Wu, P. Fu, Z. Wang, and C. Chen, Chem. Mater. **16**, 2906 (2004).
[18] W. Schnick and J. Lücke, Z. Anorg. Allg. Chem. **588**, 19 (1990).
[19] F. J. Pucher, F. Hummel, and W. Schnick, Eur. J. Inorg. Chem. **2015**, 1886 (2015).
[20] K. Landskron, S. Schmid, and W. Schnick, Z. Anorg. Allg. Chem. **627**, 2469 (2001).
[21] G. Kresse and D. Joubert, Phys. Rev. B **59**, 1758 (1999).
[22] J. P. Perdew, K. Burke, and M. Ernzerhof, Phys. Rev. Lett. **77**, 3865 (1996).
[23] G. Kresse and J. Hafner, Phys. Rev. B **47**, R558 (1993).
[24] P. Blaha, K. Schwarz, G. Madsen, D. Kvaniscka, and J. Luitz, *Wien2k, An Augmented Plane Wave Plus Local Orbitals Program for Calculating Crystal Properties* (Vienna University of Technology, Vienna, Austria, 2001).
[25] D. Koller, F. Tran, and P. Blaha, Phys. Rev. B **83**, 195134 (2011).
[26] S. Sharma and C. Ambrosch-Draxl, Phys. Scr. **T109**, 128 (2004).
[27] R. W. Nunes and X. Gonze, Phys. Rev. B **63**, 155107 (2001).
[28] X. Gonze, B. Amadon, P.-M. Anglade, J.-M. Beuken, F. Bottin, P. Boulanger, F. Bruneval, D. Caliste, R. Caracas, M. Cote, T. Deutsch, L. Genovese, Ph. Ghosez, M. Giantomassi S. Goedecker, D. R. Hamann, P. Hermet, F. Jollet, G. Jomard, S. Leroux, M. Mancini, S. Mazevet, M. J. T. Oliveira, G. Onida, Y. Pouillon, T. Rangel, G.-M. Rignanese, D. Sangalli, R. Shaltaf, M. Torrent, M. J. Verstraete, G. Zerah, and J. W. Zwanziger, Comput. Phys. Commun. **180**, 2582 (2009).
[29] F. Nastos, B. Olejnik, K. Schwarz, and J. E. Sipe, Phys. Rev. B **72**, 045223 (2005).
[30] Z. Li, Q. Liu, S. Han, T. Iitaka, H. Su, T. Tohyama, H. Jiang, Y. Dong, B. Yang, F. Zhang, Z. Yang, and S. Pan, Phys. Rev. B **93**, 245125 (2016).
[31] See Supplemental Material at http://link.aps.org/supplemental/10.1103/PhysRevMaterials.3.025201 for crystal structural parameters.
[32] J. E. Sipe and A. I. Shkrebtii, Phys. Rev. B **61**, 5337 (2000).
[33] A. Cortijo, Phys. Rev. B **94**, 235123 (2016).
[34] J. Rammer and H. Smith, Rev. Mod. Phys. Rev. **58**, 323 (1986).
[35] W.-K. Tse and A. H. MacDonald, Phys. Rev. Lett. **105**, 057401 (2010).
[36] E. I. Blount, in *Solid State Physics: Advances in Research and Applications*, Vol. 13 (Academic, New York, 1962).
[37] R. Resta, Rev. Mod. Phys. **66**, 899 (1994).
[38] R. Resta and D. Vanderbilt, in *Physics of Ferroelectrics*, edited by C. H. Ahn, K. M. Rabe, and J. M. Triscone, Topics in Applied Physics Vol. 105 (Springer-Verlag, Heidelberg, 2007), pp. 31-68.

[39] D. Xiao, M.-C. Chang, and Q. Niu, Rev. Mod. Phys. **82**, 1959 (2010).
[40] X. Jiang, S. Zhao, Z. Lin, J. Luo, P. D. Bristowe, X. Guan, and C. Chen, J. Mater. Chem. C **2**, 530 (2014).
[41] J. L. P. Hughes and J. E. Sipe, Phys. Rev. B **53**, 10751 (1996).
[42] J. E. Sipe and E. Ghahramani, Phys. Rev. B **48**, 11705 (1993).
[43] C. Aversa and J. E. Sipe, Phys. Rev. B **52**, 14636 (1995).
[44] C. Wang, X. Liu, L. Kang, B.-L. Gu, Y. Xu, and W. Duan, Phys. Rev. B **96**, 115147 (2017).
[45] T. Morimoto and N. Nagaosa, Sci. Adv. **2**, e1501524 (2016).
[46] T. Morimoto and N. Nagaosa, Phys. Rev. B **94**, 035117 (2016).
[47] B. M. Fregoso, T. Morimoto, and J. E. Moore, Phys. Rev. B **96**, 075421 (2017).
[48] R. von Baltz and W. Kraut, Phys. Rev. B **23**, 5590 (1981).
[49] I. Sodemann and L. Fu, Phys. Rev. Lett. **115**, 216806 (2015).
[50] T. Morimoto, S. Zhong, J. Orenstein, and J. E. Moore, Phys. Rev. B **94**, 245121 (2016)
[51] E. Deyo, L. E. Golub, E. L. Ivchenko, and B. Spivak, arXiv:0904.1917.
[52] Z. Li, Y.-Q. Jin, T. Tohyama, T. Iitaka, J.-X. Zhang, and H. Su, Phys. Rev. B **97**, 085201 (2018).
[53] A. Cammarata, W. Zhang, P. S. Halasyamani, and J. M. Rondinelli, Chem. Mater. **26**, 5773 (2014).
[54] A. Cammarata and J. M. Rondinelli, ACS Photonics **1**, 96 (2014).
[55] R. C. Eckardt, H. Masuda, Y. X. Fan, and R. L. Byer, IEEE J. Quantum Electron. **26**, 922 (1990).
[56] Z. S. Lin, J. Lin, Z. Z. Wang, Y. C. Wu, N. Ye, C. T. Chen, and R. K. Li, J. Phys.: Condens. Matter **13**, R369 (2001).
[57] J. Lin, M.-H. Lee, Z. P. Liu, C. Chen, and C. J. Pichard, Phys. Rev. B **60**, 13380 (1999).
[58] C.-G. Duan, J. Li, Z.-Q. Gu, and D.-S. Wang, Phys. Rev. B **59**, 369 (1999).
[59] J. Li, C.-G. Duan, Z.-Q. Gu, and D.-S. Wang, Phys. Rev. B **57**, 6925 (1998).
[60] H. Mao, F. Fu, B. Wu, and C. Chen, Appl. Phys. Lett. **61**, 1148 (1992).
[61] T. Ukachi, R. J. Lane, W. R. Bosenberg, and C. L. Tang, Appl. Phys. Lett. **57**, 980 (1990).